Strong influence of periodic boundary conditions on lateral diffusion in lipid bilayer membranes

Brian A. Camley,[1,2] Michael G. Lerner,[3,4] Richard W. Pastor,[4] and Frank L. H. Brown[2,5]
[1]*Center for Theoretical Biological Physics and Department of Physics, University of California, San Diego, California 92093, USA*
[2]*Department of Physics, University of California, Santa Barbara, California 93106, USA*
[3]*Department of Physics and Astronomy, Earlham College, Richmond, Indiana 47374, USA*
[4]*Laboratory of Computational Biology, National Heart, Lung, and Blood Institute, National Institutes of Health, Bethesda, Maryland 20892, USA*
[5]*Department of Chemistry and Biochemistry, University of California, Santa Barbara, California 93106, USA*

(Received 5 August 2015; accepted 29 September 2015; published online 16 October 2015)

The Saffman-Delbrück hydrodynamic model for lipid-bilayer membranes is modified to account for the periodic boundary conditions commonly imposed in molecular simulations. Predicted lateral diffusion coefficients for membrane-embedded solid bodies are sensitive to box shape and converge slowly to the limit of infinite box size, raising serious doubts for the prospects of using detailed simulations to accurately predict membrane-protein diffusivities and related transport properties. Estimates for the relative error associated with periodic boundary artifacts are 50% and higher for fully atomistic models in currently feasible simulation boxes. MARTINI simulations of LacY membrane protein diffusion and LacY dimer diffusion in DPPC membranes and lipid diffusion in pure DPPC bilayers support the underlying hydrodynamic model. © *2015 AIP Publishing LLC.* [http://dx.doi.org/10.1063/1.4932980]

I. INTRODUCTION

Lipid bilayer membranes and the proteins embedded within them are crucial to a wide variety of biological processes.[1] Increasingly, molecular simulations are employed in the study of the membrane surface, with models ranging from very detailed united-atom and all-atom descriptions,[2–4] to coarse-grained models with chemical specificity,[5] to aggressively coarse-grained generic lipid models in implicit solvent.[6,7] Though these models are often used to study thermodynamics, equilibrium fluctuations and rapid local dynamics of, e.g., single lipid chains, simulation studies related to transport coefficients in the membrane environment are becoming more common.[8–14] This paper cautions that diffusion coefficients for membrane-embedded objects modeled via molecular simulation may be strongly affected by finite-size effects and provides estimates for the magnitude of the problem.

Simulated diffusion coefficients for solutes in a fluid phase are known to display systematic errors that depend on system size.[15,16] These effects arise because the hydrodynamic disturbance caused by a moving object is long-ranged; in an unbounded homogeneous three-dimensional (3D) fluid, the velocity field of a translating spherical body decays only as $1/r$, where r is the distance away from the sphere (see, e.g., Ref. 17). For simulations of a solute in a homogeneous bulk fluid contained in a periodic cubic box of linear dimension $\mathcal{L}$, it is well known[15,16] that the solute diffuses more slowly than in an infinite fluid. Corrections to the infinite-system result converge to zero like $1/\mathcal{L}$ as box size is increased. Theoretically, this result may be derived via creeping flow hydrodynamics in the periodic geometry. The membrane analog to 3D creeping flow is provided by the Saffman-Delbrück (SD) model, which treats membranes as a thin viscous two-dimensional (2D) fluid layer, surrounded by a less viscous bulk.[18,19] The hydrodynamic flow around a membrane-embedded moving body in the SD model is substantially more complex than in a pure 3D fluid.[18–20] Reflecting aspects of both 2D flow within the membrane and 3D flow around the membrane, SD hydrodynamics has been described as "quasi-two-dimensional" (quasi-2D).[21] The question of how quasi-2D SD flow affects diffusion coefficients in a periodic simulation box is the primary subject of this paper.

II. SAFFMAN-DELBRÜCK HYDRODYNAMICS AND THE MEMBRANE OSEEN TENSOR FOR A PERIODIC GEOMETRY

The traditional Saffman-Delbrück model is easily extended to a membrane in a periodic geometry. This geometry, sketched in Fig. 1, includes a square $(L \times L)$ 2D fluid membrane patch with surface viscosity η_m, surrounded by a bulk fluid with viscosity η_f. The membrane is embedded in a rectangular box with periodic boundary conditions (PBCs); the total slab of simulated water has height $2H$. If $H = L/2$, the simulation box would be a cube, assuming an infinitely thin membrane. For a physical membrane of finite thickness, $H = L/2$ implies a simulation box that is longer in the z than the x,y dimensions by the thickness of the bilayer.

Appendix A demonstrates that an *in-plane* force density of $\mathbf{f}(\mathbf{r})$ applied to the membrane of Fig. 1 yields the lipid velocity

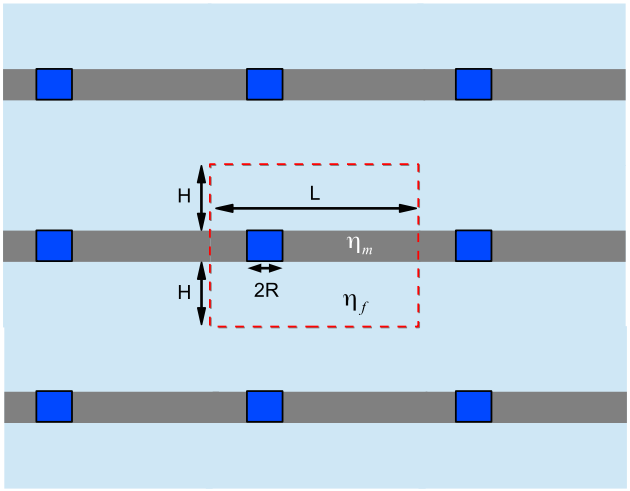

FIG. 1. Illustration of membrane model. A periodic simulation box (dashed red line) with total water thickness $2H$ and lateral dimensions $L \times L$ is assumed. The membrane is treated as an incompressible 2D fluid with surface viscosity η_m, while the surrounding incompressible fluid has viscosity η_f. The protein (or other diffusing object) is modeled as a cylinder of radius R embedded within the membrane.

field $\mathbf{v}(\mathbf{r})$ with

$$v_i(\mathbf{r}) = \int d^2r' T_{ij}^{\mathrm{PBC}}(\mathbf{r}-\mathbf{r}') f_j(\mathbf{r}'), \tag{1}$$

where we have assumed the Einstein summation convention over the x, y Cartesian coordinates indexed by i and j and the PBC membrane Oseen tensor is given by

$$T_{ij}^{\mathrm{PBC}}(\mathbf{r}) = \frac{1}{L^2} \sum_{\mathbf{k}\neq 0} T_{ij}^{\mathrm{PBC}}(\mathbf{k}) e^{-i\mathbf{k}\cdot\mathbf{r}}, \tag{2}$$

$$T_{ij}^{\mathrm{PBC}}(\mathbf{k}) = \frac{1}{\eta_m k^2 + 2\eta_f k \tanh(kH)} \left(\delta_{ij} - \frac{k_i k_j}{k^2}\right). \tag{3}$$

Note that the notation above uses identical symbols for both the real-space and Fourier-space versions of the membrane Oseen tensor; distinction between the two is indicated by the argument of the function. This convention will be followed throughout the paper. It should be stressed that Eq. (2) is not precisely a Fourier series: the sum includes only nonzero wavevectors $\mathbf{k}$, i.e., $\mathbf{k} = \frac{2\pi}{L}(m,n)$ with integer m,n, excepting $m = n = 0$. This restriction arises because the periodic system evolves with conservation of momentum and an assumed stationary center of mass—there is no net velocity in the system, so the $k = 0$ mode of velocity must be zero. Alternately, because of the stationary center of mass, the total force applied to the membrane must sum to zero. This point is discussed extensively in Refs. 15 and 16.

In the limit of $H \to \infty, L \to \infty$, the PBC membrane Oseen tensor reduces to the well-known result for an infinite system,[22,23]

$$T_{ij}^{\infty}(\mathbf{k}) = \frac{1}{\eta_m k^2 + 2\eta_f k} \left(\delta_{ij} - \frac{k_i k_j}{k^2}\right),$$

with

$$T_{ij}^{\infty}(\mathbf{r}) = \int \frac{d^2k}{(2\pi)^2} T_{ij}^{\infty}(\mathbf{k}) e^{-i\mathbf{k}\cdot\mathbf{r}}. \tag{4}$$

$T_{ij}^{\infty}(\mathbf{r})$ can be expressed in closed (but messy) form in terms of Bessel and Struve functions (see, e.g., Refs. 21 and 23). A closed form solution for the general PBC case does not seem possible.

III. PREDICTION OF DIFFUSION COEFFICIENTS IN THE PERIODIC BOX

Traditionally, the calculation of particle diffusion coefficients from a hydrodynamic theory involves solving a boundary-value problem for the Stokes flow of fluid around a steadily translating object with no-slip boundary conditions on its surface (see, e.g., Ref. 17). With the fluid velocity field in hand, the hydrodynamic drag on the particle may be calculated. The drag coefficient is the inverse of the particle mobility μ, and the diffusion coefficient follows via the Einstein relation as $D = k_B T \mu$. Unfortunately, these hydrodynamic boundary-value problems can be difficult to solve analytically. Expressions for D for simply shaped objects in 3D fluids are known,[17] but an exact solution for quasi-2D membrane geometry is known only for a circular disk in an infinite membrane surrounded by an infinite bulk (the well-known Saffman-Delbrück-Hughes-Pailthorpe-White, SDHPW, result[18–20]) and that solution is so complex that simplified functional forms are often used to approximate the true solution.[24,25] It seems highly unlikely that this expression could be generalized to the finite periodic geometry, and even if it could, the resulting equations would almost certainly be prohibitively complicated.

A practical numerical approach to the prediction of D via the immersed boundary (IB) method[26] is presented in this section. In the IB approach, solution of a complicated boundary value problem is avoided by approximating the solid diffusing object as a fluid region. Although initially developed for use in continuum level simulations of particulate suspensions, the IB scheme provides an elementary means to compute single-particle diffusion coefficients numerically.[27] In the infinite quasi-2D membrane geometry, IB calculations successfully reproduce the SDHPW diffusion coefficient.[28] IB calculations also reproduce known PBC effects on the diffusion of spherical particles in 3D[16,29] (Appendix C). It should be stressed that while IB calculations only approximate exact solutions for D of no-slip solid bodies, the approximation works very well and no-slip boundaries are themselves imperfect models of physical behavior. Further, the purpose of this paper is to explore the effects of PBC on lateral diffusion coefficients in membranes, not to attempt quantitative prediction of membrane-protein diffusion coefficients in periodic boxes. If it were possible to quantitatively predict D for real proteins, there would be no need to carry out simulations at all. If one were inclined to refine the IB calculations here to quantitatively reproduce no-slip boundary value solutions for D, methods have been introduced to do this, both in 3D[30–32] and in the membrane geometry.[33–35]

Implementing the IB scheme to calculate D is straightforward. A force density is applied to the IB "particle," assumed radially symmetric and located at the origin: $\mathbf{f}(\mathbf{r}) = \mathbf{F}\delta_R(\mathbf{r})$, where δ_R is a "finite delta" function (i.e., $\int d^2r \delta_R(\mathbf{r}) = 1$, and δ_R has a characteristic envelope size R). The velocity of the membrane-embedded object caused by this forcing is taken to

be $\mathbf{V} = \int d^2r' \mathbf{v}(\mathbf{r}')\delta_R(r')$. Without loss of generality, the force is applied in the x direction, so that $\mathbf{F} = F\hat{\mathbf{x}}$; by symmetry $\mathbf{V}$ is in the $\hat{\mathbf{x}}$ direction. It follows from Eq. (1) that $\mathbf{V} = \mu\mathbf{F}$, with the mobility given by

$$\mu = \frac{1}{L^2}\sum_{\mathbf{k}\neq 0} |\delta_R(\mathbf{k})|^2 T_{xx}^{PBC}(\mathbf{k}). \tag{5}$$

The diffusion coefficient is, by the Einstein relation, $D = k_B T\mu$.

For convenience, $\delta_R(\mathbf{r})$ is chosen to be a Gaussian. The width of $\delta_R(\mathbf{r})$ is chosen to yield good correspondence with the SDHPW results in the infinite-system-size limit, for a cylinder with radius R. The choice $\delta_R = \frac{1}{\pi b^2} e^{-r^2/b^2}$ with $b = \beta R$ and $\beta = 0.828\,494$[36] reproduces the SDHPW result[19,20,24,25] to within 6% over the entire range $10^{-5} \leq R/L_{sd} \leq 10^5$ (here, $L_{sd} = \eta_m/2\eta_f$ is the Saffman-Delbrück length). With this choice,

$$D^{\mathrm{PBC}} = \frac{k_B T}{2L^2}\sum_{\mathbf{k}\neq 0} \frac{1}{\eta_m k^2 + 2\eta_f k \tanh(kH)} e^{-k^2\beta^2 R^2/2}. \tag{6}$$

By comparison, in an infinite system ($L \to \infty$, $H \to \infty$),

$$D^{\infty} = \frac{k_B T}{2}\int \frac{d^2k}{(2\pi)^2} \frac{1}{\eta_m k^2 + 2\eta_f k} e^{-k^2\beta^2 R^2/2}. \tag{7}$$

Results (6) and (7) apply to membrane-spanning cylinders of radius R and are expected to be appropriate for capturing the behavior of transmembrane proteins. These expressions may be generalized to cylinders that span only a single leaflet of the bilayer as a crude model for monotopic proteins or lipids; see Appendix B. The numerical examples in the body of this paper will focus on the transmembrane case, with lipid diffusion considered separately in Appendix B.

Eq. (6) is the primary theoretical result of this paper, and we will spend the remainder of this section exploring its implications. While the series in Eq. (6) cannot be summed analytically, numerical summation is straightforward, since the integrand vanishes exponentially for $k \gg 1/R$. In addition, some important consequences of PBC on D can be gleaned directly from inspection of Eq. (6). Consider the summand of Eq. (6). In the small-k (large wavelength) limit, it asymptotically approaches $\left[(\eta_m + 2\eta_f H)k^2\right]^{-1}$; this suggests that at wavelengths long compared to H, the combination of membrane and surrounding periodic fluid acts as a single two-dimensional fluid with surface viscosity $\eta_m + 2\eta_f H$. It is thus expected for D^{PBC} to diverge logarithmically with L as $L \to \infty$ with H fixed, in analogy to the pure 2D case[18] (i.e., the Stokes paradox). This behavior is demonstrated explicitly in Fig. 2. (As noted in Refs. 18 and 19, inertial effects should eventually regulate this divergence for macroscopic values of L, but this is not expected to be relevant for boxes on the order of microns or smaller. Including the effects of non-zero Reynolds numbers into mobility calculations can be difficult;[37] to our knowledge, no systematic attempt to do this for the membrane geometry has been made.)

From Eqs. (6) and (7), the relative error in D due to periodic confinement, $(D^{\mathrm{PBC}} - D^{\infty})/D^{\infty}$, depends on H, L, and R only in terms of the unitless variables H/L_{sd}, L/L_{sd}, and R/L_{sd}; errors are thus expected to be small if both L and H exceed L_{sd}. What is the Saffman-Delbrück length for a typical simulated bilayer system? In the case of fully atomistic simulations, molecular architectures are faithfully represented and one expects L_{sd} to closely mimic experimental values. Experimental measurements of L_{sd} for lipid bilayer systems are typically in the 100 nm to micron range.[24,25,38–42] In coarse-grained models, some details of lipid and solvent structure are lost and there is no reason to expect close correspondence to experimental numbers. For example, in the coarse-grained MARTINI force field,[5] η_m has been determined to be 1.2×10^{-8} P cm for DPPC bilayers, with water viscosity $\eta_f = 7 \times 10^{-3}$ P.[9] Within MARTINI simulations, we expect $L_{sd} \approx 8.6$ nm—much smaller than the experimental range. United-atom simulations lead to results intermediate between experiment and MARTINI.[43]

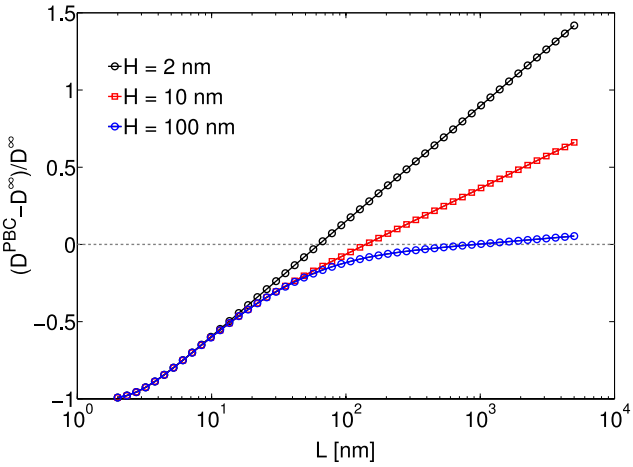

FIG. 2. Varying the lateral system size L without changing the height H leads to systematic errors in the measured diffusion coefficient. Although increasing L has the effect of raising D to approach infinite-system results in small systems, the growth of D is unbounded and asymptotically grows logarithmically in L to eventually overshoot the infinite-system results. $R = 1$ nm and the MARTINI DPPC value of $L_{sd} = 8.6$ nm is assumed.

Fig. 3 plots the predicted relative error in D as a function of H and L for parameters appropriate to both MARTINI simulations ($L_{sd} = 8.6$ nm) and all-atom simulations. ($L_{sd} = 78$ nm as suggested by the experiments of Ref. 40 involving proteins of different sizes diffusing on black lipid membranes. This value is among the lowest reported in the experimental literature—$L_{sd} = 163$ nm was measured by Ref. 44, and much larger numbers have also been reported.[45] $L_{sd} = 78$ nm serves as a conservative estimate for the purposes of this paper; larger values of L_{sd} exacerbate the errors associated with PBC.) The data are presented for a small protein of radius 1 nm, but similar results are obtained for larger R. Table I lists numerical predictions for D for a few representative transmembrane proteins using parameters appropriate to typical all-atom and MARTINI simulations. Errors associated solely with PBC conditions range from 30% to 80%, with the errors being larger for big proteins and for all-atom simulations. Of course the MARTINI simulations are expected to introduce other (larger) sources of absolute error relative to experiment owing to the incorrect viscosities present in the simulations.

Figs. 2 and 3 and Table I paint a bleak picture for those that would hope to extract quantitative membrane-protein diffusivities directly from molecular simulations. For representative all-atom numbers, D^{PBC} can be less than 1/4

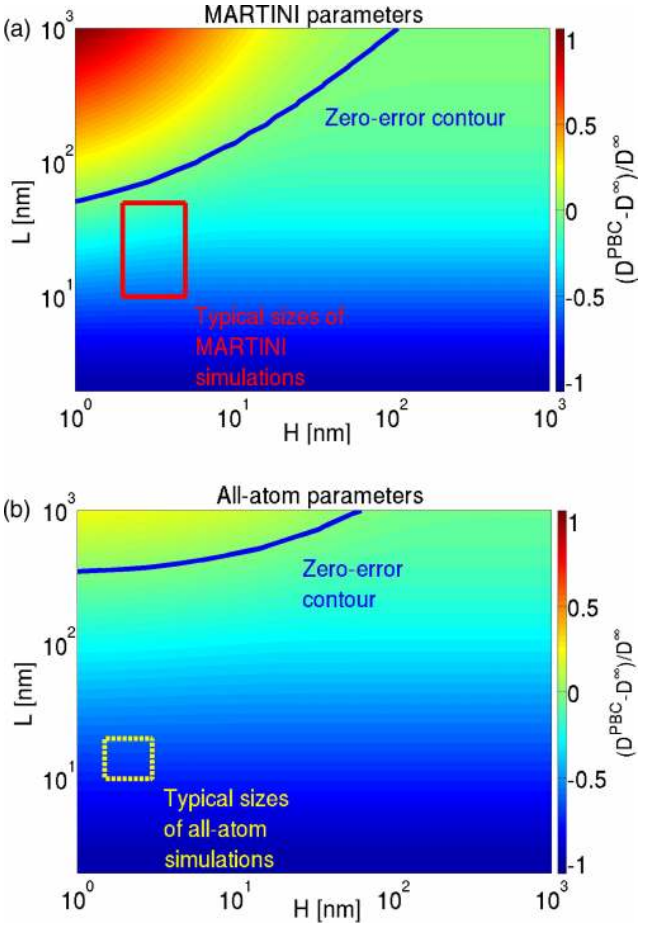

FIG. 3. In a periodic membrane simulation, the observed diffusion coefficient may be significantly larger or smaller than the value in an infinite system, D^{∞}. (a) Ranges of errors in diffusion coefficients appropriate for coarse-grained simulations (MARTINI). The solid box indicates a typical range of MARTINI simulation sizes, L ranging from 10 to 50 nm, and H ranging from 2-5 nm (H is *half* the total water height. See Fig. 1). $L_{sd} = 8.6$ nm for MARTINI. The protein radius assumed is $R = 1$ nm. (b) Errors predicted for all-atom simulations with experimentally accurate viscosities. $L_{sd} = 78$ nm as in the experiments of Ref. 40. A typical range of all-atom simulation sizes with H from 1.5 to 3 nm, and L from 10 to 20 nm is indicated by the yellow dashed box. The protein radius $R = 1$ nm in both plots. The zero-error contour is plotted to emphasize the fact that both positive and negative differences between D^{PBC} and D^{∞} can be observed depending on box geometry.

the infinite system value. In fact, the situation is likely even worse, since the value $L_{sd} = 78$ nm[40] assumed for experimental membrane systems is conservative—most measurements find larger values for L_{sd}.[24,25,38,39] The errors associated with fully atomistic boxes will only increase for larger values of L_{sd}. The errors inherent to PBC are less severe in the case of MARTINI simulations, due to both the smaller L_{sd} in MARTINI and the larger system sizes tractable to simulation; however, D^{PBC} can still be as small as 40% of D^{∞}. (It should always be remembered that MARTINI D^{∞} can be larger than experimental results by nearly an order of magnitude due to the unphysically low L_{sd} values. This point is clear in the absolute numbers of Table I but is lost in the relative errors plotted in Figs. 2 and 3.)

TABLE I. Predicted diffusion coefficients in typical PBC box geometries (Eq. (6)) and in infinite systems (Eq. (7)) for three representative proteins. For MARTINI simulations, $H = 5$ nm, $L = 25$ nm, $\eta_m = 1.2 \times 10^{-8}$ P cm, and $L_{sd} = 8.6$ nm. For all-atom simulations, $H = 2$ nm, $L = 15$ nm, $\eta_m = 1.5 \times 10^{-7}$ P cm, and $L_{sd} = 78$ nm (viscosity values chosen to match experiments of Ref. 40). $T = 323$ K in both calculations.

Protein	Radius (nm)	D^{∞} (all-atom) (10^{-7} cm^2/s)	D^{PBC} (all-atom) (10^{-7} cm^2/s)	D^{∞} (MARTINI) (10^{-7} cm^2/s)	D^{PBC} (MARTINI) (10^{-7} cm^2/s)
WALP23	0.5	1.25	0.63	9.31	6.79
LacY	2	0.93	0.31	5.63	3.12
GltT	4	0.77	0.16	4.03	1.56

A point of particular concern involves the logarithmic growth of D^{PBC} with L at fixed H, seen in Fig. 2. It is a common practice in molecular simulations to include minimal cushions of water around the membrane in an attempt to minimize computational expense spent on solvent while modeling as large a membrane patch as possible. Waters are added around the membrane to the point of full hydration of the bilayer, or perhaps slightly beyond this point, leading to simulation boxes that are anisotropic with larger lateral dimensions (L) than the normal dimension (H). Though this strategy may be adequate for modeling many thermodynamic observables and fluctuations, it is very clear that this could be a disastrous protocol for modeling lateral transport in the membrane. Following such a way of thinking, one would naively seek to converge simulation results by increasing the membrane size L, while keeping the cushion of water around the membrane constant (i.e., constant H). Repeating simulations at ever larger values of L, D^{PBC} will simply grow without bound, passing through D^{∞} as the zero error contour of Fig. 3 is crossed and continuing on to infinitely large values. Although Fig. 3 might seem to indicate that one could simply choose L to lie on the zero error curve to reproduce D^{∞} exactly, the curve itself can only be drawn with a prior knowledge of D^{∞}.

To be sure, it is theoretically possible to converge simulation results to the limit of an infinite box, but this requires both H and L to significantly exceed L_{sd}. The physical reasoning behind this assertion is that at wavelengths below L_{sd}, a quasi-2D membrane behaves essentially as a 2D system—which will have a system size dependence of $\ln L$. It is only for lengths beyond L_{sd} that the membrane begins to lose sufficient momentum to its surroundings that a more traditional 3D hydrodynamic behavior is observed.[18] However, this crossover at L_{sd} in lateral dimensions presumes a sufficient cushion of water surrounding the membrane to accept this transmitted momentum and not return it to the membrane. In the infinite system, it can be shown that the fluid flows in the bulk around the membrane decay exponentially away from the membrane with the same lengthscale as the wavelength of the flow within the membrane itself.[22,23] In other words, to see the expected crossover to 3D-like behavior for lateral dimensions of L_{sd}, there should also be a cushion of water surrounding the membrane comparable to or larger than L_{sd}. To quantify these qualitative ideas, Fig. 4 plots the relative errors in D as a function of box size while holding the ratio H/L constant. Unlike Fig. 2, moving to the right on the x-axis on this plot corresponds to increasing both L and H simultaneously. It is observed that increasing H and L simultaneously will generally lead to convergence to the infinite system size results. However, depending on the

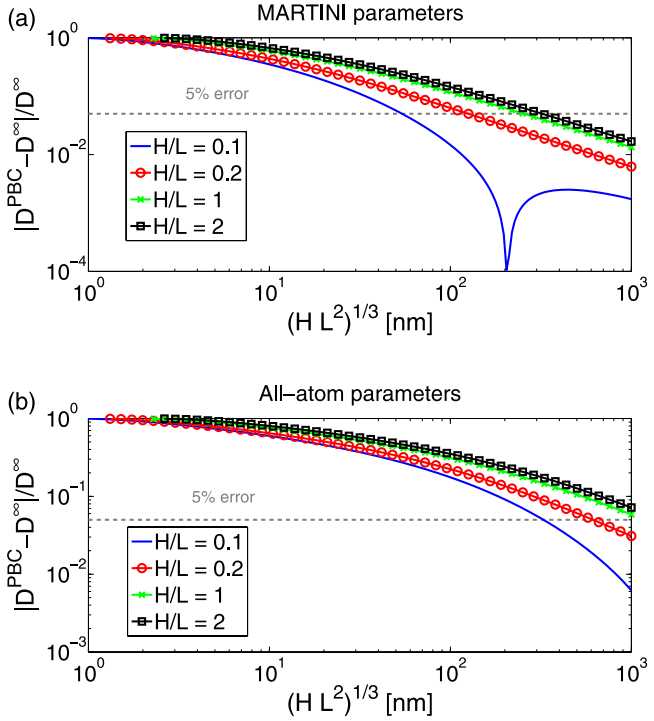

FIG. 4. Simultaneously increasing L and H leads to a decrease in absolute percentage error between periodic simulations and the infinite-system limit. Here, $(HL^2)^{1/3}$ is used as a measure of the nominal linear "size" of the simulation on the x-axis for various fixed ratios of H to L. If linear scaling is assumed, computational cost will grow like HL^2; converging the simulations to the indicated 5% error tolerance would require system sizes well beyond those currently possible on today's computers. The same parameters are used as in Fig. 3. The non-monotonic behavior of the blue curve in the MARTINI pane indicates an accidental coincidence between D^{PBC} and D^{∞} at a particular box geometry, i.e., the system has passed through the "zero-error contour" of Fig. 3.

ratio H/L, this convergence can be faster or slower, and may even be non-monotonic. As is apparent in Figs. 2 and 3 above, box shape has a strong influence on D^{PBC}, which can create accidental coincidences with the infinite system size result at finite box sizes in specific geometries—but only in the limit of both H and L large will the results truly converge. This convergence only occurs at relatively large system sizes. To converge a MARTINI simulation of a 1 nm protein within 5% error of the infinite system size, assuming $H/L = 0.1$ (our best case in Fig. 4), we would need $L \approx 115$ nm and $H \approx 11.5$ nm. This is a factor of 8 larger in volume than typically applied simulations. The situation is far worse in all-atom computations, where the required sizes for 5% error would be roughly $L \approx 700$ nm and $H \approx 70$ nm—a completely unreasonable size for today's computers, but an unavoidable conclusion dictated by the physically relevant value of $L_{sd} = 78$ nm assumed in the plot. Again, it is stressed that $L_{sd} = 78$ nm represents the low end of measurements for the Saffman-Delbrück length. If L_{sd} is closer to the micron scale, as reported in some experiments,[24,25,38,39,45] the required box sizes would be even larger.

There would not appear to be a direct and straightforward way to infer D^{∞} solely based on finite size simulations. In principle, one could imagine fitting multiple simulations over varied box geometries to Eq. (6) in order to obtain the hydrodynamic parameters of the model (η_f, η_m, R). In turn, these parameters could be used to estimate D^{∞} via Eq. (7). As a matter of practice, it seems likely that such a scheme would be difficult to implement and could be problematic if the hydrodynamic theory of Eqs. (6) and (7) fails to account for all the necessary physics in the system (see Sec. VI).

IV. DIMERS OF PROTEINS

Knight *et al.* have recently studied the diffusion of dimers of membrane-bound proteins,[10] observing both experimentally and in molecular dynamics simulations that diffusion coefficients of protein dimers are half that of individual proteins. This implies that the hydrodynamic correlations between the two proteins are negligible, i.e., they are freely draining. Two of us recently showed that the strength of these correlations strongly depends on the hydrodynamic environment of the membrane, with particular focus paid to the influence of a solid supporting substrate beneath the bilayer.[34] In this section, it is shown that PBC can also change hydrodynamic correlations significantly, and that quantitative comparison between experiment and simulations of membrane dimer diffusion must consider the effects of PBC.

To calculate the diffusion coefficient of a protein dimer (as illustrated in Fig. 5), the mobility of the assembly in directions parallel to $(\mu_{\parallel})$ and perpendicular to $(\mu_{\perp})$ its long axis must be computed. Without loss of generality, the dimer's long axis is assumed coincident with the x direction. Applying a steady total force $F\hat{\mathbf{x}}$ to the dimer ($F\hat{\mathbf{x}}/2$ to each monomer), the dimer will move with a constant velocity $\mathbf{v} = \mu_{\parallel} F\hat{\mathbf{x}}$. Considering either protein, its velocity will include a contribution $\mu^{\mathrm{monomer}} F/2\hat{\mathbf{x}}$ from the direct force on that protein and a contribution of $T_{xx}(\mathbf{r})F/2$, where T_{xx} is the membrane Oseen tensor and $\mathbf{r}$ the separation of the proteins. (This description, which approximates the hydrodynamic correlations between the monomers in the point-particle approximation, should be regarded as a quasi-2D version of the Kirkwood

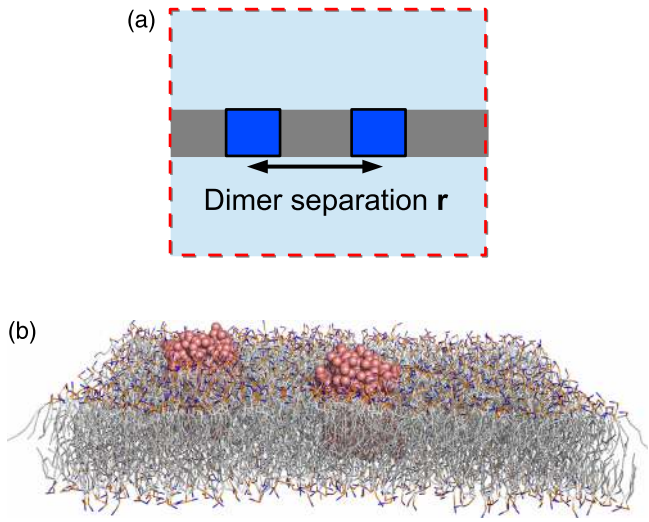

FIG. 5. (a) Illustration of dimer of proteins separated by distance $\mathbf{r}$ within simulation box; periodic boundary conditions are assumed but not shown. (b) Snapshot of representative frame of simulation of LacY dimer within a MARTINI DPPC bilayer.

approximation.[31,33]) Thus, $\mu_{\parallel} = \frac{1}{2}\left[\mu^{\text{monomer}} + T_{xx}(\mathbf{r})\right]$;[34,35,46] the dimer diffusion coefficient approaches half the monomer diffusion coefficient only when the hydrodynamic correlations, represented by the membrane Oseen tensor, are negligible. Similarly, $\mu_{\perp} = \frac{1}{2}\left[\mu^{\text{monomer}} + T_{yy}(\mathbf{r})\right]$. Though the dimer will have different diffusion coefficients along its two axes ($D_{\parallel} = k_B T \mu_{\parallel}$, $D_{\perp} = k_B T \mu_{\perp}$), in the long time limit its center of mass will diffuse with an isotropic diffusion coefficient $D^{\text{dimer}} = \left[D_{\parallel} + D_{\perp}\right]/2$ owing to rotational averaging.[47] Therefore, the long-time, rotationally averaged diffusion coefficient of a protein dimer with separation $\mathbf{r}$ is

$$D^{\text{dimer}} = \frac{1}{2}\left[D^{\text{monomer}} + k_B T \;\bar{T}(\mathbf{r})\right], \tag{8}$$

where $\bar{T}(\mathbf{r}) = \frac{1}{2}\text{tr}\, T_{ij}(\mathbf{r}) = \frac{1}{2}\left[T_{xx}(\mathbf{r}) + T_{yy}(\mathbf{r})\right]$ and $\mathbf{r}$ is the center-center separation of the protein dimer. This result applies generally to both the PBC and infinite case. Differences between the two result from the different values for both monomer diffusion and the membrane Oseen tensor between the two hydrodynamic geometries. The Kirkwood approximation will break down in the limit where the separation $\mathbf{r}$ approaches the size of the protein;[34,35] in fact, $\bar{T}(\mathbf{r})$ diverges as $\mathbf{r} \to 0$. For numerical simplicity in converging the sum in Eq. (2), a regularized Oseen tensor is used,[34] multiplying the integrand of Eq. (2) by $\phi_\epsilon(\mathbf{r}) = \frac{1}{2\pi\epsilon^2} e^{-r^2/2\epsilon^2}$ with $\epsilon = 0.3$ nm; it was verified that this does not affect any of the results shown.

Predicted dimer diffusion coefficients for an imagined MARTINI simulation are shown in Fig. 6. The dimer-monomer ratio is seen to depend strongly on system size. In particular, for commonly used system sizes, the hydrodynamic correlation can drop to zero or even become negative at separations of 4-5 nm, and therefore the dimer diffusion coefficient can drop below half of the monomer diffusion coefficient—representing an *anticorrelation* between the motion of two proteins at certain separations. This suggests that dimer simulations in MARTINI[10] could potentially observe an apparent absence of correlations due to PBC, even if the Saffman-Delbrück model would predict strong correlations in the infinite system. It should be noted that if r is comparable to L, $\bar{T}^{PBC}(\mathbf{r})$ is noticeably anisotropic; Fig. 6 considers only the orientationally averaged results.

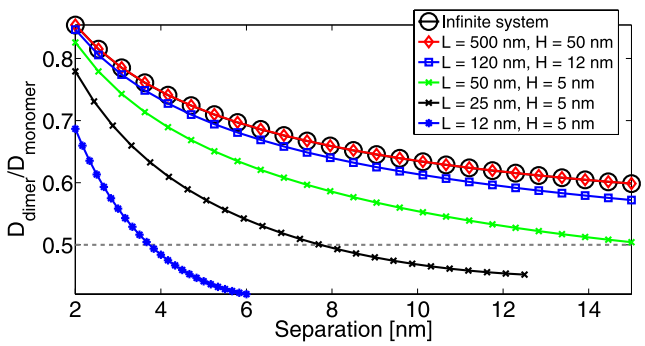

FIG. 6. Diffusion coefficients of a dimer of proteins with radius $R = 1$ nm in the Kirkwood approximation (Eq. (8)). D_{monomer} is computed via Eq. (6) for the given system size, and this plot assumes the typical MARTINI value of $L_{sd} = 8.6$ nm. Results reflect an average over orientation within the simulation box (see text). Only separations with $r < L/2$ are plotted.

Fig. 6 also illustrates that the dimer/monomer ratio will eventually converge to the result for an infinite system, but that this takes very large system sizes, of the order of hundreds of nanometers. This is comparable to the system sizes required to converge the monomer diffusion coefficients, as studied above.

V. MARTINI SIMULATIONS OF TRANSMEMBRANE PROTEIN DIFFUSION: MONOMER AND DIMERS

To assess the predictions of Secs. II–IV, simulations of the membrane spanning protein LacY (Fig. 5(b)) were run in the MARTINI coarse-grained force field[5,48,49] using GROMACS 4.0.5.[50] Both monomers and dimers were studied; the dimers are connected by stiff harmonic constraints with equilibrium lengths of 6 and 10 nm and a force constant of 1250 kJ mol^{-1} nm^{-2}. This spring connects the CA bead of Pro123 on one LacY monomer to the CA bead of Pro123 on the other; these are the beads closest to the LacY center.

All systems contained 2048 DPPC lipids and 50 784 waters and were simulated at a temperature of 323 K with a Nosé-Hoover thermostat[51,52] and Parrinello-Rahman barostat.[53] Although this integrator is not ideal for studying hydrodynamic effects,[54,55] attempts to implement strict energy and momentum conserving simulations within GROMACS were not successful and were ultimately abandoned. While use of the NPT thermostat is recognized to be a potential issue, the below results do seem to indicate support for the predictions in Secs. II–IV.

To set up the initial lipid bilayers, the procedure used in Knight *et al.*[10] was followed. The bilayers equilibrated to $L = 25.0$ nm with water height $H = 5.1$ nm and a membrane thickness of 4 nm (i.e., total z-dimension box size of 14.2 nm). 25 starting conformations were chosen from equally spaced coordinate sets in the last 1/4 of a microsecond equilibration for each of the systems. New velocities were assigned, and each of these was run for 1.8 μs of NPT. The first 100 ns of each simulation was considered equilibration and the final 1.7 μs as production.

The starting configuration and force field parameters for LacY were taken from the CGDB.[49] PyMOL[56] was used to manually align LacY with one of the pre-equilibrated 2048-lipid bilayer systems. After adding counterions and deleting overlapping waters and lipids, the system was energy minimized and run for 1 μs at NPT. The same procedure was followed for LacY dimers separated by 6 and 10 nm. All three systems were then simulated as described above, yielding 75 trajectories and 127.5 μs of production. Diffusion coefficients were determined by fitting to the mean square displacements of the LacY monomer or LacY dimer center of masses.

Diffusion coefficients for monomeric LacY and the two dimers (6 nm and 10 nm separations) were found to be $D_{\text{monomer}} = (2.06 \pm 0.19) \times 10^{-7}$ cm^2/s, D_{dimer} (6 nm) $= (1.33 \pm 0.19) \times 10^{-7}$ cm^2/s, and D_{dimer} (10 nm) $= (1.16 \pm 0.11) \times 10^{-7}$ cm^2/s, respectively.[57] To compare these data with theory, η_m for MARTINI DPPC was treated as a fitting

constant in Eq. (6) to reproduce the simulated value of D_{monomer}. The remaining constants were held to the values specified above: $H = 5.1$ nm, $L = 25.0$ nm, $R = 2$ nm, and $\eta_f = 7 \times 10^{-3}$ P. The resulting best-fit $\eta_m = 1.99 \times 10^{-8}$ P cm, which is reasonably close to the value previously reported in the literature: 1.2×10^{-8} P cm.[9] Although the disparity between the best-fit η_m and the literature value might trouble some, it is important to recognize that there are many sources for possible inconsistency between continuum theories and dynamics at the molecular level. Both length scales H and R are poorly defined on the molecular scale; it is unclear if these sizes should reflect the bare sizes of the bilayer and protein (as we have done), or some larger effective "hydrodynamic" lengths incorporating solvating layers of water around the bilayer and/or solvation shells of lipids around the protein. Beyond this, if LacY causes a distortion of the lipids and/or waters in its immediate vicinity, this will lead to further ambiguities in the hydrodynamic parameters. The literature value of viscosity for MARTINI DPPC is based on a single measurement of an isolated homogeneous lipid system without protein inclusions,[9] which is expected to need some refinement for application to the present system if all other parameters are taken as fixed. Using $\eta_m = 1.99 \times 10^{-8}$ P cm along with the other fixed parameters in Eq. (8) leads to the theoretical predictions for dimer diffusivities in Fig. 7 (blue curve). The predictions are in reasonable agreement with the simulated D_{dimer} values.

If one were to attempt to fit the simulated data assuming an infinite box theory—i.e., just repeat the procedures of the above paragraph, but interpret the simulations as if $H = L = \infty$ using Eq. (7) for the η_m fit—the resulting value for $\eta_m^{\infty} = 5.71 \times 10^{-8}$ P cm. This value is in considerably worse agreement with the literature precedent than is the value from the PBC fit, which in itself might discredit use of the infinite theory. Furthermore, the subsequent theoretical prediction for dimer diffusion based on the infinite geometry (red dashed curve in Fig. 7) appears inconsistent with the simulations. There are obvious serious limitations when one attempts to use hydrodynamic theory for quantitative predictions at the ~nm scale, but the simulations do seem to indicate a clear influence of PBC artifacts.

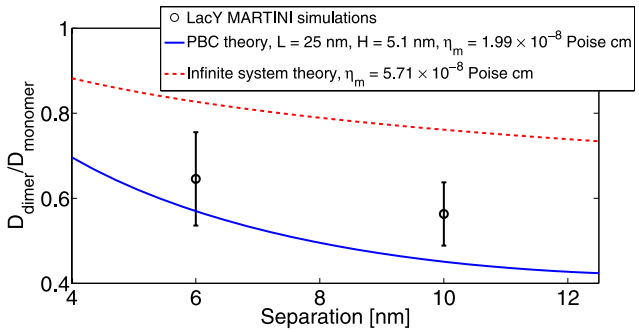

FIG. 7. Simulations of LacY dimer diffusion in a lipid bilayer membrane are consistent with a theory including PBC, but not one neglecting those effects. The viscosities presented are determined by fitting to the simulated monomer diffusion coefficient $D_{\text{monomer}} = 2.06 \times 10^{-7}$ cm^2/s (see text). We have averaged our theory over orientation within the simulation box, as in Fig. 6.

VI. DISCUSSION

Throughout this work, the validity of the Saffman-Delbrück hydrodynamic model is assumed. With this assumption follows the unavoidable conclusion that strong size-dependent effects should influence simulations of lipid bilayer membranes that aim to study lateral transport. Though we believe the Saffman-Delbrück picture to be largely correct, we highlight a few potential issues that may limit the quantitative applicability of our conclusions. The following points are discussed in the paragraphs below: (1) simulations without momentum conservation are not expected to agree with hydrodynamic theories like Saffman-Delbrück, (2) the Saffman-Delbrück model assumes creeping flow, completely neglecting inertia, (3) at the small scales of proteins and lipids, continuum models may break down, (4) the membrane's undulations may alter diffusion coefficients, and (5) non-hydrodynamic sources of dissipation may be important, especially if proteins distort the membrane.

1. The Saffman-Delbrück model is a hydrodynamic model that assumes momentum conservation. This assumption is violated in some common molecular dynamics algorithms. For example, in Langevin dynamics, each particle is subjected to a frictional drag and a stochastic force obeying a fluctuation-dissipation theorem (see, e.g., Ref. 58). This additional friction force significantly changes the hydrodynamics of a simulated fluid,[29] and one should not expect either the present results or the SDHPW results to hold in Langevin dynamics simulations. Other thermostats, including the commonly used Nosé-Hoover approach, may also potentially disrupt hydrodynamic flows.[54,55] To study transport properties, either an NVE integrator or a thermostat specifically designed to preserve hydrodynamics (e.g., dissipative particle dynamics thermostats[59,60]) would be most appropriate. Unfortunately, most large-scale simulation packages suitable for studying realistic lipid architectures do not support this functionality without some degree of modification and tinkering. A robust test of the theories presented here will require further simulations.
2. The Saffman-Delbrück model and its extensions here assume the Stokes limit, where the inertia of the membrane and surrounding fluid are completely neglected. Certain aspects of our predictions, particularly the 2D-like divergence of D with L at fixed H, would likely be modified with the inclusion of inertial effects. In a true 2D fluid, the Reynolds number is a singular perturbation[37] that can regularize similar divergences and we expect that analogous effects may apply to our PBC quasi-2D geometry. However, extension of Stokes limit diffusion coefficient calculations to nonzero Reynolds number can be quite difficult. We know of no systematic attempts to treat this for the membrane geometry.
3. Saffman-Delbrück approaches assume a continuum model for the membrane, which is normally only valid for objects much larger than the dimensions of the constituent molecules. Membrane proteins typically have radii in the nm scale, while the lipid head radius is around 0.5 nm, which could cause one to be uneasy about

continuum hydrodynamic models (see, e.g., Refs. 41 and 61). Even if the hydrodynamic approach is reasonable for proteins, one might be more skeptical about its use to analyze finite size effects solely for lipids.[12] Molecular dynamics simulations of the diffusion of spherical objects in fluid show that the Stokes-Einstein result with slip boundary conditions is recovered for smooth solutes four times larger than the solvent particle,[62] and stick boundary conditions can be recovered from rough solutes in some cases.[63,64] Some of these non-continuum effects may not be as relevant for membrane proteins as for spherical solutes, as the Saffman-Delbrück model predicts relatively modest changes between slip and stick boundary conditions.[18,19] Though this problem has been extensively studied in three dimensions, we are unaware of any attempts to treat it for membranes. Highly coarse-grained molecular dynamics simulations have claimed agreement with Saffman-Delbrück,[8] but determining any non-continuum effects would be difficult without both accounting for the finite size effects we describe here and independently measuring the membrane and surrounding fluid viscosities.

4. The Saffman-Delbrück model and our work assume a perfectly flat bilayer, neglecting membrane undulations. Over a sufficiently rough surface, the projected diffusion coefficient may differ from the real one.[65,66] In addition, distortions in the membrane could potentially influence hydrodynamics,[11] though to linear order in-plane and out-of-plane membrane dynamics are believed to be uncoupled.[23]
5. Finally, if a protein distorts the surrounding membrane, additional drag may be caused, reducing the protein's diffusion coefficient.[66–70] If these effects are strong enough, they could potentially compete with or even overwhelm the hydrodynamic contributions to D discussed in this work.

Above caveats notwithstanding, if the Saffman-Delbrück model is correct in essence, our system size predictions follow naturally. The mentioned complications are not anticipated to drastically modify these predictions unless the assumptions of the Saffman-Delbrück model are flagrantly violated, e.g., by using Langevin dynamics with a large friction.[29] Testing these system size effects in simulations may provide a validation of the Saffman-Delbrück assumptions, without having to deal with the complications arising from varying protein sizes, as done experimentally.[40,44,71] Even if Saffman-Delbruck predictions are not fully accurate in the description of experiment, as claimed by some,[71,72] this does not mean that hydrodynamic flows are irrelevant to the self-diffusion of proteins and/or lipids in the bilayer. For example, even within the context of non-continuum "free area" theories for lipid diffusion, hydrodynamic traction from the surrounding water may still influence diffusivities.[61] In such a case, PBC would still be expected to influence lipid diffusivity, even though the predictions of Appendix B may be quantitatively off.

In addition to single-particle self-diffusion, many other physical phenomena subject to hydrodynamic flow in the membrane should be influenced by PBC. An important example has been discussed already: hydrodynamic correlations, which influence the diffusion coefficients of dimers. Using the periodic Oseen tensor will also quantitatively change the correlations measured in two-particle microrheology[73,74] in membranes. Hydrodynamic effects also arise in the long time tails of objects in fluids[28,75,76] and may be affected by PBC. Rates of protein association in three dimensions are known to depend on hydrodynamic interactions,[77,78] suggesting that associations at the membrane surface may also be sensitive to hydrodynamics and subject to PBC artifacts. However, not all hydrodynamic phenomena are expected to be as strongly influenced by PBC as self-diffusion. In computing membrane-protein mobility, the flows are very long-ranged because of the underlying force monopole. Properties controlled by higher-order force moments (e.g., rotational diffusion,[18] domain relaxation,[38] or increased intrinsic viscosity[21,70]) are expected to be less sensitive to finite system sizes.

Though this study has focused on changes in membrane hydrodynamics with finite system sizes, some of these effects may show up in three-dimensional isotropic fluids in strongly anisotropic boxes. If fluid flow is essentially uniform over the z direction, the fluid will again be nearly two-dimensional (as in the 2D-3D transition in soap films[79]), and the divergence of D with increasing L may appear.

The approaches discussed here are easily extended to various complications in membrane geometry (e.g., supported lipid bilayers[34]). A particularly relevant case involves including the two-leaflet structure of the bilayer explicitly; friction between the two leaflets then can influence the dynamics of bodies localized within a single leaflet, such as a monotopic protein or individual lipid.[34,80–82] A generalization to the two-leaflet case is provided in Appendix B. Should these single-leaflet results be applied to lipids? As discussed above, there are good reasons to be skeptical of a hydrodynamic theory applied at the scale of individual lipids, at least for quantitative predictions. However, simulations of lipids in varying box sizes qualitatively agree with theoretical predictions. Specifically, increasing L systematically increases the diffusion coefficient of lipids (Appendix B). This suggests that many of the qualitative features described here (large errors, systematic changes with $D \sim \ln L$) may be relevant to pure lipid systems and calls into question the reliability of simulation estimates for lipid self-diffusion (see Refs. 12–14 and references within).

ACKNOWLEDGMENTS

We thank Edward Lyman and Klaus Gawrisch for helpful discussions, and Antti-Pekka Hynninen for assistance with incorporating the MARTINI potential into CHARMM. This work was supported in part by the NSF (Grant Nos. CHE-1153096, CHE-1465162, and CC*IIE-1440689) and by the Intramural Research Program of the NIH, National Heart, Lung and Blood Institute, and utilized the high-performance computational capabilities at the National Institutes of Health, Bethesda, MD (NHLBI LoBoS cluster). BAC was supported in part by NIH Grant No. F32GM110983.

APPENDIX A: OSEEN TENSOR FOR A MEMBRANE WITH PERIODIC BOUNDARY CONDITIONS IN *x*, *y*, AND *z*

We want to solve the membrane Stokes equations with periodic boundary conditions in x, y, and z. The fluid above and below the membrane obeys the incompressible Stokes equations

$$\eta_f \nabla^2 \mathbf{v}_f^{\pm} - \nabla P_f^{\pm} = 0, \tag{A1}$$

$$\nabla \cdot \mathbf{v}_f^{\pm} = 0. \tag{A2}$$

The velocity of the fluid above the membrane matches the velocity at the membrane—this implies that $\mathbf{v}_f(\mathbf{r}_\perp, z = 0) = \mathbf{v}_m(\mathbf{r}_\perp)$ where $\mathbf{v}_m(\mathbf{r}_\perp)$ is the membrane velocity at $\mathbf{r}_\perp = (x, y)$. We assume that the membrane velocity $\mathbf{v}_m$ is only in the xy plane, $\mathbf{v}_m(\mathbf{r}_\perp) = (v_{m,x}, v_{m,y}, 0)$. Because of the periodic boundary conditions in z, we must have $\mathbf{v}_f^+(\mathbf{r}_\perp, z = H) = \mathbf{v}_f^-(\mathbf{r}_\perp, z = -H)$, or equivalently that $\mathbf{v}_f^+(\mathbf{r}_\perp, z = 2H) = \mathbf{v}_f^+(\mathbf{r}_\perp, z = 0) = \mathbf{v}_m(\mathbf{r}_\perp)$, and a similar constraint on $\mathbf{v}_f^-$. $\mathbf{v}_f$ must also obey periodic boundary conditions in x and y, $\mathbf{v}_f^{\pm}(x = L/2, y, z) = \mathbf{v}_f^{\pm}(x = -L/2, y, z)$ and $\mathbf{v}_f^{\pm}(x, y = L/2, z) = \mathbf{v}_f^{\pm}(x, y = -L/2, z)$.

The membrane obeys the equations

$$\eta_m \nabla^2 \mathbf{v}_m - \nabla P_m + \Pi^+ \cdot \hat{\mathbf{n}}^+ + \Pi^- \cdot \hat{\mathbf{n}}^- + \mathbf{f}(\mathbf{r}_\perp) = 0, \tag{A3}$$

$$\nabla \cdot \mathbf{v}_m = 0, \tag{A4}$$

where $\Pi^{\pm}$ is the stress tensor of the fluid above (below) the membrane, $\Pi_{ij}^{\pm} = \eta_f \left(\partial_i v_{f,j} + \partial_j v_{f,i}\right) - P_m \delta_{ij}$, $\hat{\mathbf{n}}^{\pm}$ are the upper (lower) normals to the membrane, and $\mathbf{f}(\mathbf{r}_\perp)$ is a force applied to the membrane. Here, i and j run over x,y, and z. We assume that the membrane is flat, i.e., $\hat{\mathbf{n}}^{\pm} = \pm\hat{\mathbf{z}}$ and that the membrane velocity is only in the plane—therefore, $\Pi^+ \cdot \hat{\mathbf{n}}^+ = \eta_f \partial_z \mathbf{v}_f^+(\mathbf{r}_\perp, z)|_{z=0}$. By the symmetry of the problem, $\Pi^- \cdot \hat{\mathbf{n}}^- = -\eta_f \partial_z \mathbf{v}_f^-(\mathbf{r}_\perp, z)|_{z=0} = \Pi^+ \cdot \hat{\mathbf{n}}^+$.

Because $\mathbf{v}_m$ must obey periodic boundary conditions in x and y, we can expand $\mathbf{v}_m$ in a Fourier series,

$$\mathbf{v}_m = \frac{1}{L^2} \sum_{\mathbf{q}} \mathbf{v}_m(\mathbf{q}) e^{-i\mathbf{q}\cdot\mathbf{r}_\perp}, \tag{A5}$$

where the sum is over $\mathbf{q} = (m, n, 0)\frac{2\pi}{L}$ where m and n are integers.

We will take the Ansatz that

$$\mathbf{v}_f^+(x, y, z) = \mathbf{v}_m(x, y) f(z). \tag{A6}$$

With this Ansatz, $\mathbf{v}_f^+$ is incompressible in three dimensions as long as $\mathbf{v}_m$ is incompressible in the plane. Because we have assumed a Fourier series form for $\mathbf{v}_m$, both $\mathbf{v}_m$ and $\mathbf{v}_f^+$ will satisfy the periodic boundary conditions in x and y. To ensure that $\mathbf{v}_f^+(\mathbf{r}_\perp, z = 2H) = \mathbf{v}_f^+(\mathbf{r}_\perp, z = 0) = \mathbf{v}_m(\mathbf{r}_\perp)$, we must have $f(0) = f(2H) = 1$. We must only ensure that our Ansatz solves the Stokes equations in the bulk fluid, Eq. (A1). Taking the curl of Eq. (A1) to eliminate the pressure, we find $\nabla^2 \left(\nabla \times \mathbf{v}_f^+\right) = 0$; taking the z component of this equation, we find

$$\frac{1}{L^2} \sum_{\mathbf{q}} e^{-i\mathbf{q}\cdot\mathbf{r}_\perp} \left[f''(z) - q^2 f(z)\right] \tag{A7}$$

$$\times \left[-iq_x \mathbf{v}_m(\mathbf{q}) \cdot \hat{\mathbf{y}} + iq_y \mathbf{v}_m(\mathbf{q}) \cdot \hat{\mathbf{x}}\right] = 0, \tag{A8}$$

and therefore $f''(z) = q^2 f(z)$, requiring $f(z) = A(q)e^{-qz} + B(q)e^{qz}$. Applying the boundary conditions $f(0) = 1$, $f(2H) = 1$, we find

$$f(z) = \cosh\left[q(H - z)\right] \operatorname{sech}\left[Hq\right]. \tag{A9}$$

This allows us to calculate the traction from the outside fluid on the membrane,

$$\Pi^+ \cdot \hat{\mathbf{n}}^+ = \eta_f \partial_z \mathbf{v}_f^+(\mathbf{r}_\perp, z)|_{z=0} \tag{A10}$$

$$= \frac{1}{L^2} \sum_{\mathbf{q}} \left[\eta_f f'(z = 0)\right] \mathbf{v}_m(\mathbf{q}) e^{-i\mathbf{q}\cdot\mathbf{r}_\perp} \tag{A11}$$

$$= \frac{1}{L^2} \sum_{\mathbf{q}} \left[-\eta_f q \tanh\left(qH\right)\right] \mathbf{v}_m(\mathbf{q}) e^{-i\mathbf{q}\cdot\mathbf{r}_\perp}. \tag{A12}$$

The other traction follows similarly. If we look at the Fourier transform of Eq. (A3), we thus find

$$-\eta_m q^2 \mathbf{v}_m(\mathbf{q}) - i\mathbf{q} P_m(\mathbf{q}) - 2\eta_f q \tanh(qH) \mathbf{v}_m(\mathbf{q}) + \mathbf{f}(\mathbf{q}) = 0. \tag{A13}$$

We may solve this equation and eliminate the pressure by applying the projection operator $\wp_{ij}^{\perp}(\mathbf{q}) \equiv (\delta_{ij} - q_i q_j / q^2)$; by incompressibility, $\nabla \cdot \mathbf{v}_m = 0$ and thus $\mathbf{q} \cdot \mathbf{v}_m(\mathbf{q}) = 0$ and $\wp^{\perp} \mathbf{v}_m(\mathbf{q}) = \mathbf{v}_m(\mathbf{q})$. We find

$$v_{m,i} = T_{ij}(\mathbf{q}) f_j(\mathbf{q}), \tag{A14}$$

with $T_{ij}(\mathbf{q})$ given by Eq. (3).

APPENDIX B: GENERALIZATION TO MONOTOPIC PROTEINS AND LIPIDS

The results of Section III and Appendix A are easily generalized to describe the behavior of objects embedded within only one leaflet of the membrane. Using an elementary model for two-leaflet bilayers,[34] it is found that

$$D^{\mathrm{PBC}} = \frac{k_B T}{2L^2} \sum_{\mathbf{k} \neq 0} \frac{A(k)}{A(k)^2 - B(k)^2} e^{-k^2\beta^2 R^2/2}, \tag{B1}$$

$$D^{\infty} = \frac{k_B T}{2} \int \frac{d^2k}{(2\pi)^2} \frac{A(k)}{A(k)^2 - B(k)^2} e^{-k^2\beta^2 R^2/2}, \tag{B2}$$

$$A(k) = \eta_{\mathrm{mono}} k^2 + \eta_f k \coth(2Hk) + b, \tag{B3}$$

$$B(k) = b + \eta_f k \operatorname{csch}(2Hk), \tag{B4}$$

where b is the intermonolayer friction coefficient and $\eta_{\mathrm{mono}} = \eta_m/2$ is the monolayer surface viscosity. It is readily verified that in the limit $b \to \infty$, Eqs. (B1) and (B2) reproduce Eqs. (6) and (7).

Figure 8 displays the predicted relative error in D for a single-leaflet or "monotopic" body approximately the size of a lipid or small peptide ($R = 0.5$ nm). The results are qualitatively similar to Fig. 3: the logarithmic divergence at large L for fixed H persists, as does the convergence to infinite-box results when $H, L \gg L_{sd}$. However, the complex interplay between viscosities, intermonolayer friction, and box geometry does lead to some quantitative differences with Fig. 8. The most obvious of these differences is the relatively small disparity between the MARTINI and all-atom cases (panes (a) and (b)) as compared to the bilayer-spanning example displayed in Fig. 3. This is not a general

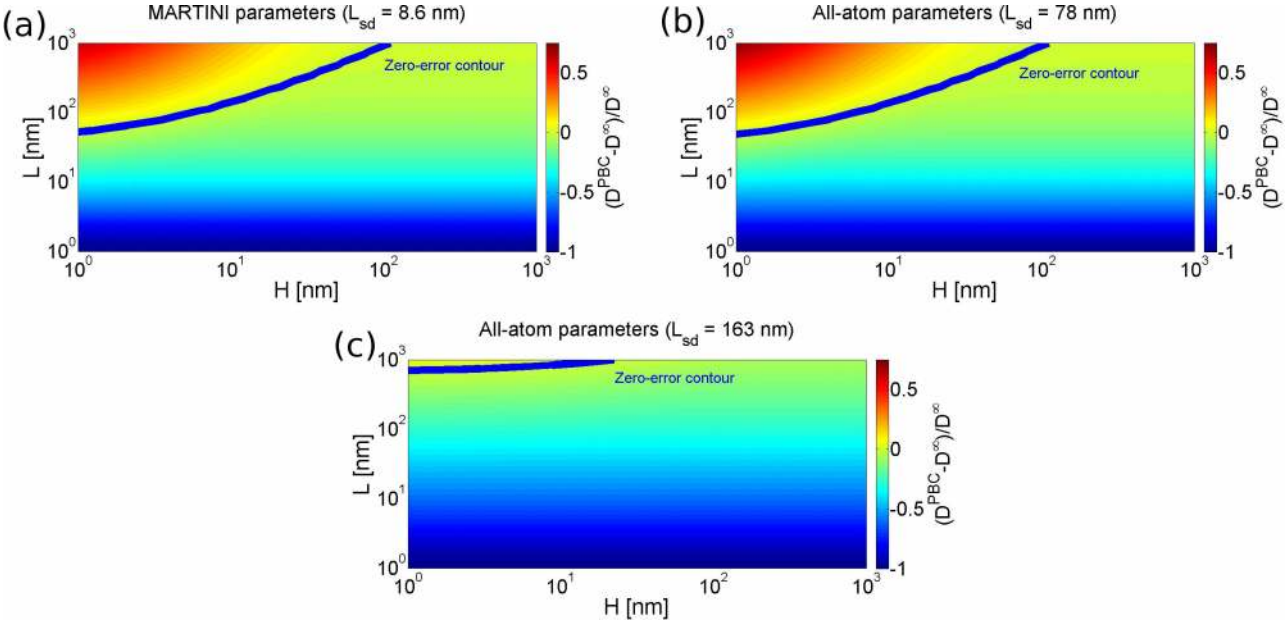

FIG. 8. The influence of PBC on a monotopic object (Eq. (B1), displayed here) is qualitatively similar to that of a membrane-spanning object (Eq. (6), see Fig. 3). (a) Errors in diffusion coefficients appropriate for coarse-grained simulations (MARTINI), with membrane monolayer viscosity $\eta_{\rm mono} = 6\times10^{-9}$ P cm and $\eta_f = 0.007$ P ($L_{sd} = 8.6$ nm), and interleaflet friction coefficient $b = 2.4\times10^5$ P/cm.[9] (b) Errors in diffusion coefficients appropriate for all-atom simulations, with viscosities set to match that of Ref. 40, $\eta_{\rm mono} = 7.5\times10^{-8}$ P cm, $\eta_f = 0.0096$ P ($L_{sd} = 78$ nm), and interleaflet friction $b = 10^7$ P/cm (a representative physical value; see Ref. 34 and references within). (c) Errors in diffusion coefficients appropriate for all-atom simulations, with viscosities set to match that of Ref. 44, $\eta_{\rm mono} = 1.63\times10^{-7}$ P cm, $\eta_f = 0.01$ P ($L_{sd} = 163$ nm), and interleaflet friction $b = 10^7$ P/cm. The object radius assumed is $R = 0.5$ nm in all plots, corresponding to a small peptide or lipid. The zero-error contour is plotted to emphasize the fact that both positive and negative differences between $D^{\rm PBC}$ and D^{∞} can be observed depending on box geometry.

consequence of single-leaflet particles but results from the particular numerical values used for the monolayer viscosity and intermonolayer friction. To make this point clear, an additional pane (c) is included, using a different estimate of $L_{sd} = 163$ nm, which is also experimentally motivated.[44] Indeed, as discussed previously, the value $L_{sd} = 78$ nm is among the lowest reported in the experimental literature; $L_{sd} = 163$ nm can be considered closer to a consensus value and it is likely that pane (c) of Fig. 8 provides a more accurate prediction of all-atom simulations than does pane (b).

As mentioned in Sec. VI, there are obvious reasons to question the direct application of Eq. (B1) to lipids. However, preliminary simulations of lipid diffusion appear qualitatively consistent with the hydrodynamic model; these results are briefly summarized here. Eight MARTINI DPPC bilayer simulations to compare both the effects of box size/geometry and MD integrators (NPT vs NVE) were carried out. Given our previously mentioned inability to implement strictly energy-conserving simulations within GROMACS, the systems were pre-equilibrated in GROMACS and run for production in CHARMM.[83] The MARTINI force field uses a cosine-based angle potential; this was implemented using DOMDEC[84] for fast parallel computation within CHARMM that would be exactly comparable to GROMACS. DPPC bilayers were set up following the procedure in the work of Knight *et al.*[10] Four equilibrated bilayers were prepared in GROMACS, with L = 12.7 nm and H = 4.85 nm, L = 25.4 nm and H = 4.85 nm, L = 12.7 nm and H = 9.70 nm, and L = 25.4 nm and H = 9.70 nm, all with a membrane thickness of 4.0 nm. These systems were simulated at a temperature of 323 K with Parrinello-Rahman semi-isotropic pressure coupling and Nosé-Hoover temperature coupling. New velocities were assigned, and these were run for 2.3, 1.0, 2.5, and 1.0 μs of NPT, respectively. Each system was then resized to fit into a tetragonal unit cell and further equilibrated for 2 ns in CHARMM using extended system pressure coupling and Nosé-Hoover temperature coupling to maintain a pressure of 1 atm and a temperature of 323 K. Those four equilibrated bilayers were used to start eight production runs (four NPT and four NVE), with total production times shown in Table II. Diffusion coefficients were obtained by fitting to the linear portion of the mean square displacement curve. Standard errors were obtained by block averaging, with ten blocks per simulation.

The molecular dynamics simulations of MARTINI DPPC lipids within CHARMM display qualitative, though not quantitative agreement with Eq. (B1) (see Table II). As quantitative agreement is not expected between simulation and

TABLE II. Comparison of lipid diffusion coefficients in MARTINI simulations to the predictions of Eq. (B1). In qualitative agreement with Eq. (B1) at the studied box geometries, increasing L causes significant increases in simulated lipid diffusivity, but increasing H has little effect.

L (nm)	H (nm)	D, theory (10^{-7} cm^2/s)	D, NVE MARTINI (10^{-7} cm^2/s)	D, NPT MARTINI (10^{-7} cm^2/s)	Simulation time (μs) NVE/NPT
12.7	4.85	8.51	7.65 ± 0.2	8.14 ± 0.1	6.9/6.6
25.4	4.85	10.1	9.52 ± 0.2	10.2 ± 0.2	2.0/1.9
12.7	9.7	8.51	7.99 ± 0.2	8.57 ± 0.2	4.8/3.7
25.4	9.7	9.99	9.85 ± 0.2	9.83 ± 0.2	1.7/1.8

hydrodynamic theory for lipids, no attempt has been made to fit the parameters ($\eta_{\rm mono}$, b) of Eq. (B1) in comparison to the simulations. Rather, the nominal MARTINI DPPC values reported in Ref. 9 were used, as detailed in Fig. 8.

APPENDIX C: RELATION WITH PREVIOUS APPROACHES: THE IMMERSED BOUNDARY METHOD REPRODUCES KNOWN RESULTS IN 3D

We compare the immersed-boundary approach to known results in three dimensions. Yeh and Hummer[16] claim in 3D that, for a sphere of radius R in a three-dimensional box of linear size $\mathcal{L}$ with fluid of viscosity η,

$$D_{\rm 3D}^{\rm PBC} = D_{\rm 3D}^{\infty} - \frac{k_B T}{6\pi\eta\mathcal{L}}\left(\xi - \frac{4\pi R^2}{3\mathcal{L}^2}\right), \tag{C1}$$

where $\xi \approx 2.837\,297$.

We will show that the immersed-boundary approach reproduces Eq. (C1) very accurately, as long as the relationship between the immersed boundary object size a and the sphere radius R is calibrated appropriately. First, we compute the immersed-boundary result for the mobility in a three-dimensional infinite system, with an immersed-boundary Gaussian of size a; we will address the relationship between a and R below

$$\mu_{\rm 3D}^{\infty} = \int \frac{d^3k}{(2\pi)^3}\frac{e^{-k^2a^2}}{\eta k^2}\left(1 - \frac{k_z k_z}{k^2}\right) \tag{C2}$$

$$= \frac{2}{3}\int \frac{d^3k}{(2\pi)^3}\frac{e^{-k^2a^2}}{\eta k^2} \tag{C3}$$

$$= \frac{1}{6\pi^{3/2}\eta a}. \tag{C4}$$

We see here that we get the correct Stokes-Einstein scaling $\mu \sim 1/\eta a$ (a result similar to that obtained in Ref. 85). If we require $\mu = [6\pi\eta R]^{-1}$, we find that $R = \sqrt{\pi}a$, i.e., the immersed boundary object with size parameter a corresponds with a no-slip object of $R > a$. (We use a slightly different convention for the size parameter here; above, we have written our equations in terms of $b = \sqrt{2}a$.)

In cubic periodic boundary conditions with a linear size $\mathcal{L}$, the immersed-boundary result is

$$\mu_{\rm 3D}^{\rm PBC} = \frac{1}{\mathcal{L}^3}\sum_{\mathbf{k}\neq 0}\frac{e^{-k^2a^2}}{\eta k^2}\left(1 - \frac{k_z k_z}{k^2}\right), \tag{C5}$$

where the sum is over $\mathbf{k} = \frac{2\pi}{\mathcal{L}}(m,n,p)$ with m,n,p varying over all integers (aside from $m = n = p = 0$). We can cast this into the form

$$\mu_{\rm 3D}^{\rm PBC} = \frac{1}{\eta a}\frac{2}{3}\frac{\alpha}{(2\pi)^3}\sum_{m,n,p}{}' \frac{e^{-(m^2+n^2+p^2)\alpha^2}}{m^2+n^2+p^2}, \tag{C6}$$

where the prime indicates the exclusion of $m = n = p = 0$ and $\alpha = 2\pi a/\mathcal{L}$. As $\alpha \to 0$, Eq. (C6) approaches Eq. (C4). What should the finite-size corrections look like? From Eq. (C1), if we assume that $R = \gamma a$, we expect

$$\left[\mu_{\rm 3D}^{\rm PBC} - \mu_{\rm 3D}^{\infty}\right] = \Delta\mu^{(1)} + \Delta\mu^{(2)}, \tag{C7}$$

where

$$\eta a \Delta\mu^{(1)} = -\frac{\xi}{12\pi^2}\alpha, \tag{C8}$$

$$\eta a \Delta\mu^{(2)} = \frac{2}{9}\gamma^2\frac{\alpha^3}{(2\pi)^3}. \tag{C9}$$

We show that this is the case in Fig. 9 by plotting $\eta a \mu_{\rm 3D}^{\rm PBC} - \eta a \mu_{\rm 3D}^{\infty} + \frac{\xi}{12\pi^2}\alpha$ as a function of α. In fact, we find that the "effective radius" of $R = \sqrt{\pi}a$ ($\gamma = \sqrt{\pi}$), as motivated by the comparison to an infinite-volume Stokes mobility above, is a very good fit for the residual error; the best fit is $R = 0.977\sqrt{\pi}a$. This corresponds to saying $b = \beta R$ in three dimensions, with $\beta \approx \frac{\sqrt{2}}{0.977\pi} \approx 0.82$—surprisingly close to the value found for the membrane geometry above ($\beta = 0.828\,494$).

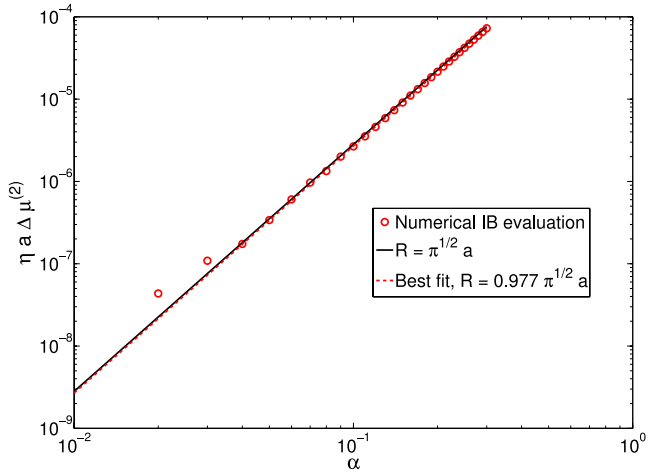

FIG. 9. Second correction to the mobility, $\eta a \Delta\mu^{(2)} = \eta a \mu_{\rm 3D}^{\rm PBC} - \eta a \mu_{\rm 3D}^{\infty} + \frac{\xi}{12\pi^2}\alpha$. $\eta a \mu_{\rm 3D}^{\rm PBC}$ is calculated from Eq. (C6); the sum is calculated over the range $n,m,p \in [-n_{\rm max}, n_{\rm max}]$ where $n_{\rm max} = \lfloor 4/\alpha \rfloor$ ($\lfloor \cdots \rfloor$ is the floor function). These values of $n_{\rm max}$ are sufficient to ensure convergence.

[1] R. B. Gennis, *Biomembranes: Molecular Structure and Function* (Springer-Verlag, Berlin, 1989).
[2] J. B. Klauda, R. M. Venable, J. A. Freites, J. W. O'Connor, D. J. Tobias, C. Mondragon-Ramirez, I. Vorobyov, A. D. MacKerell, Jr., and R. W. Pastor, J. Phys. Chem. B **114**, 7830 (2010).
[3] L. Rosso and I. R. Gould, J. Comput. Chem. **29**, 24 (2008).
[4] O. Berger, O. Edholm, and F. Jähnig, Biophys. J. **72**, 2002 (1997).
[5] S. Marrink, H. Risselada, S. Yefimov, D. Tieleman, and A. De Vries, J. Phys. Chem. B **111**, 7812 (2007).
[6] I. R. Cooke, K. Kremer, and M. Deserno, Phys. Rev. E **72**, 011506 (2005).
[7] G. Brannigan, L. C.-L. Lin, and F. L. Brown, Eur. Biophys. J. **35**, 104 (2006).
[8] G. Guigas and M. Weiss, Biophys. J. **91**, 2393 (2006).
[9] W. den Otter and S. Shkulipa, Biophys. J. **93**, 423 (2007).
[10] J. Knight, M. Lerner, J. Marcano-Velázquez, R. Pastor, and J. Falke, Biophys. J. **99**, 2879 (2010).
[11] M. Chavent, T. Reddy, J. Goose, A. C. E. Dahl, J. E. Stone, B. Jobard, and M. S. Sansom, Faraday Discuss. **169**, 455 (2014).
[12] J. B. Klauda, B. R. Brooks, and R. W. Pastor, J. Chem. Phys. **125**, 144710 (2006).
[13] E. Flenner, J. Das, M. C. Rheinstädter, and I. Kosztin, Phys. Rev. E **79**, 011907 (2009).
[14] T. Apajalahti, P. Niemelä, P. N. Govindan, M. S. Miettinen, E. Salonen, S.-J. Marrink, and I. Vattulainen, Faraday Discuss. **144**, 411 (2010).
[15] B. Dünweg and K. Kremer, J. Chem. Phys. **99**, 6983 (1993).
[16] I.-C. Yeh and G. Hummer, J. Phys. Chem. B **108**, 15873 (2004).
[17] S. Kim and S. J. Karrila, *Microhydrodynamics: Principles and Selected Applications* (Dover Publications, 2005).

[18]P. G. Saffman and M. Delbrück, Proc. Natl. Acad. Sci. U. S. A. **72**, 3111 (1975).
[19]P. Saffman, J. Fluid Mech. **73**, 593 (1976).
[20]B. D. Hughes, B. A. Pailthorpe, and L. R. White, J. Fluid Mech. **110**, 349 (1981).
[21]N. Oppenheimer and H. Diamant, Biophys. J. **96**, 3041 (2009).
[22]D. K. Lubensky and R. E. Goldstein, Phys. Fluids **8**, 843 (1996).
[23]A. J. Levine and F. C. MacKintosh, Phys. Rev. E **66**, 061606 (2002).
[24]E. P. Petrov and P. Schwille, Biophys. J. **94**, L41 (2008).
[25]E. P. Petrov, R. Petrosyan, and P. Schwille, Soft Matter **8**, 7552 (2012).
[26]C. Peskin, Acta Numer. **11**, 1 (2002).
[27]P. J. Atzberger, Phys. Lett. A **351**, 225 (2006).
[28]B. A. Camley and F. L. H. Brown, Phys. Rev. E **84**, 021904 (2011).
[29]B. Dünweg, J. Chem. Phys. **99**, 6977 (1993).
[30]A. J. Levine and T. C. Lubensky, Phys. Rev. E **63**, 041510 (2001).
[31]M. Doi and S. F. Edwards, *The Theory of Polymer Dynamics* (Clarendon Press, 1999).
[32]R. Cortez, SIAM J. Sci. Comput. **23**, 1204 (2001).
[33]A. J. Levine, T. B. Liverpool, and F. C. MacKintosh, Phys. Rev. E **69**, 021503 (2004).
[34]B. A. Camley and F. L. Brown, Soft Matter **9**, 4767 (2013).
[35]E. Noruzifar, B. A. Camley, and F. L. Brown, J. Chem. Phys. **141**, 124711 (2014).
[36]This value is not precisely the one that we used in Ref. 28, which was $\beta = 0.797\,91$. The value for β used in this paper was fitted to the corrected Saffman-Delbrück interpolation presented in Ref. 25, as the one developed in Ref. 24 and used for our earlier paper has a typo.
[37]J. Veysey II and N. Goldenfeld, Rev. Mod. Phys. **79**, 883 (2007).
[38]B. A. Camley, C. Esposito, T. Baumgart, and F. L. H. Brown, Biophys. J. **99**, L44 (2010).
[39]A. R. Honerkamp-Smith, F. G. Woodhouse, V. Kantsler, and R. E. Goldstein, Phys. Rev. Lett. **111**, 038103 (2013).
[40]K. Weiß, A. Neef, Q. Van, S. Kramer, I. Gregor, and J. Enderlein, Biophys. J. **105**, 455 (2013).
[41]W. L. Vaz, F. Goodsaid-Zalduondo, and K. Jacobson, FEBS Lett. **174**, 199 (1984).
[42]Y. A. Domanov, S. Aimon, G. E. Toombes, M. Renner, F. Quemeneur, A. Triller, M. S. Turner, and P. Bassereau, Proc. Natl. Acad. Sci. U. S. A. **108**, 12605 (2011).
[43]T. J. Müller and F. Müller-Plathe, ChemPhysChem **10**, 2305 (2009).
[44]S. Ramadurai, A. Holt, V. Krasnikov, G. Van Den Bogaart, J. Killian, and B. Poolman, J. Am. Chem. Soc. **131**, 12650 (2009).
[45]T. T. Hormel, S. Q. Kurihara, M. K. Brennan, M. C. Wozniak, and R. Parthasarathy, Phys. Rev. Lett. **112**, 188101 (2014).
[46]This brief derivation provides the correct result, but has ignored the forces of constraint associated with the dimer. A rigorous derivation may be found in Section V of Ref. 35.
[47]Y. Han, A. Alsayed, M. Nobili, J. Zhang, T. Lubensky, and A. Yodh, Science **314**, 626 (2006).
[48]L. Monticelli, S. Kandasamy, X. Periole, R. Larson, D. Tieleman, and S. Marrink, J. Chem. Theory Comput. **4**, 819 (2008).
[49]M. Sansom, K. Scott, and P. Bond, Biochem. Soc. Trans. **36**, 27 (2008).
[50]B. Hess, C. Kutzner, D. Van Der Spoel, and E. Lindahl, J. Chem. Theory Comput. **4**, 435 (2008).
[51]S. Nosé, J. Chem. Phys. **81**, 511 (1984).
[52]W. G. Hoover, Phys. Rev. A **31**, 1695 (1985).
[53]M. Parrinello and A. Rahman, J. Appl. Phys. **52**, 7182 (1981).
[54]D. Frenkel and B. Smit, *Understanding Molecular Simulation: From Algorithms to Applications* (Academic Press, 2001), Vol. 1.
[55]S. D. Stoyanov and R. D. Groot, J. Chem. Phys. **122**, 114112 (2005).
[56]Schroedinger, LLC, The PyMOL Molecular Graphics System, Version 1.4.1, 2011.
[57]In computing these diffusion coefficients, bilayer center of mass motion was removed. Trajectories were converted from GROMACS to CHARMM format, and CHARMM's correl command was used to calculate MSD curves. Diffusion coefficients were obtained by fitting to the linear portion of the MSD curve.
[58]G. S. Grest and K. Kremer, Phys. Rev. A **33**, 3628 (1986).
[59]R. D. Groot and P. B. Warren, J. Chem. Phys. **107**, 4423 (1997).
[60]T. Soddemann, B. Dünweg, and K. Kremer, Phys. Rev. E **68**, 046702 (2003).
[61]W. L. Vaz, R. M. Clegg, and D. Hallmann, Biochemistry **24**, 781 (1985).
[62]F. Ould-Kaddour and D. Levesque, Phys. Rev. E **63**, 011205 (2000).
[63]J. Schmidt and J. Skinner, J. Phys. Chem. B **108**, 6767 (2004).
[64]J. Schmidt and J. Skinner, J. Chem. Phys. **119**, 8062 (2003).
[65]A. Naji and F. L. Brown, J. Chem. Phys. **126**, 235103 (2007).
[66]A. Naji, P. Atzberger, and F. L. H. Brown, Phys. Rev. Lett. **102**, 138102 (2009).
[67]A. Naji, A. J. Levine, and P. Pincus, Biophys. J. **93**, L49 (2007).
[68]B. A. Camley and F. L. Brown, Phys. Rev. E **85**, 061921 (2012).
[69]V. Démery and D. S. Dean, Phys. Rev. E **84**, 011148 (2011).
[70]B. A. Camley and F. L. Brown, J. Chem. Phys. **141**, 075103 (2014).
[71]Y. Gambin, R. Lopez-Esparza, M. Reffay, E. Sierecki, N. S. Gov, M. Genest, R. S. Hodes, and W. Urbach, Proc. Natl. Acad. Sci. U. S. A. **103**, 2098 (2006).
[72]Y. Gambin, M. Reffay, E. Sierecki, F. Homblé, R. S. Hodges, N. S. Gov, N. Taulier, and W. Urbach, J. Phys. Chem. B **114**, 3559 (2010).
[73]A. J. Levine and T. C. Lubensky, Phys. Rev. E **65**, 011501 (2001).
[74]V. Prasad, S. Koehler, and E. Weeks, Phys. Rev. Lett. **97**, 176001 (2006).
[75]R. Zwanzig and M. Bixon, Phys. Rev. A **2**, 2005 (1970).
[76]B. Alder and T. Wainwright, Phys. Rev. A **1**, 18 (1970).
[77]D. Brune and S. Kim, Proc. Natl. Acad. Sci. U. S. A. **91**, 2930 (1994).
[78]J. Antosiewicz and J. A. McCammon, Biophys. J. **69**, 57 (1995).
[79]V. Prasad and E. R. Weeks, Phys. Rev. Lett. **102**, 178302 (2009).
[80]K. Seki, S. Mogre, and S. Komura, Phys. Rev. E **89**, 022713 (2014).
[81]T. Han, T. P. Bailey, and M. Haataja, Phys. Rev. E **89**, 032717 (2014).
[82]R. J. Hill and C.-Y. Wang, Proc. R. Soc. A **470**, 20130843 (2014).
[83]B. R. Brooks, C. L. Brooks, A. D. MacKerell, L. Nilsson, R. J. Petrella, B. Roux, Y. Won, G. Archontis, C. Bartels, S. Boresch *et al.*, J. Comput. Chem. **30**, 1545 (2009).
[84]A.-P. Hynninen and M. F. Crowley, J. Comput. Chem. **35**, 406 (2014).
[85]P. J. Atzberger, P. R. Kramer, and C. S. Peskin, J. Comput. Phys. **224**, 1255 (2007).